Available online at www.sciencedirect.com
ScienceDirect
Trans. Nonferrous Met. Soc. China 25(2015) 2701−2707
Transactions of Nonferrous Metals Society of China
www.tnmsc.cn

Prediction of vulnerable zones based on residual stress and microstructure in CMT welded aluminum alloy joint

Feng-yuan SHU[1,2], Ze TIAN[1], Yao-hui LÜ[2], Wen-xiong HE[1], Fei-yang LÜ[1], Jian-jun LIN[2,3], Hong-yun ZHAO[1], Bin-shi XU[2]

1. Shandong Provincial Key Laboratory of Special Welding Technology, School of Materials Science and Engineering, Harbin Institute of Technology at Weihai, Weihai 264209, China;
2. National Key Laboratory for Remanufacturing, Academy of Armored Forces Engineering, Beijing 100072, China;
3. Shanghai Key Laboratory of Materials Laser Processing and Modification, Shanghai Jiao Tong University, Shanghai 200240, China

Received 22 December 2013; accepted 28 May 2015

Abstract: Numerical simulation and experimental results were employed for the identification of the most vulnerable zones in three-pass cold-metal-transferring (CMT) welded joint. The residual stress distribution in the joint was predicted by finite element (FE) method, while the structural morphology of distinctive zones was obtained through metallographic experiments. The highest principal stress made the symmetric face of the joint most sensitive to tensile cracks under service conditions. Whereas, the boundaries between the weld seam and the base plates were sensitive to cracks because the equivalent von Mises stress was the highest when the first interpass cooling was finished. The third weld pass and the inter-pass remelted zones exhibited the modest mechanical performances as a result of the coarse grain and coarse grain boundary, respectively. The most vulnerable zones were regarded to be the crossed parts between the zones identified by numerical and experimental methods.

Key words: aluminum alloy; vulnerable zone; cold-metal-transferring welded joint; residual stress; microstructure morphology

1 Introduction

The relative location of the vulnerable zones in the welded joint could be obtained through destructive experiments including tensile test, impact test and fatigue test. Tensile test was mostly used and often followed by microstructure analysis. HUANG et al [1] studied the gas tungsten arc (GTA) welded AA7A52 plates and found that tensile cracks initiated in the weld seam and 18 mm away from the center of the weld seam. Transmission electron microscopy (TEM) results were then employed to reveal the mechanism. However, destructive experiments were often of high cost and time consuming. The importance of numerical method lay upon the prediction of test results and assistance to theoretical demonstration in addition to lower cost [2]. Combination of the numerical and experimental methods made an efficient way for materials science. FU et al [3] studied the mechanical behaviors of pulsed gas metal arc (GMA) welded AA7005 plates by experiments and numerical methods. It was found that the softened zone covered the area within 12 mm from the weld pool boundary.

With regard to the vulnerable zones in aluminum alloy welded joints, MA and OUDEN [4] studied the softening of HAZ in the welded AA7020 and AA7022 joints. The HAZ was divided into the quenched zone and the overaging zone in which the strengthening phase was dissolved and got coarser, respectively, which was in strict consistence with Refs. [1,3,5]. This was supposed to be the mechanism of softening in HAZ. It was also found that the hardness over the HAZ could be retained by artificial post weld heat treatment which was more effective than natural aging. Different research results were also reported. MA et al [6] performed standard tensile tests on the plasma arc (PA) welded AA7A52 joints. The tensile rupture occurred in the weld seam in which equiaxed grains and strip-shaped grains were found simultaneously. The weld seam was also reported [7] as the weakest zone in the twin-wire GMA

Foundation item: Project (9140C850205120C8501) supported by the Major Program of State Key Laboratory of Remanufacturing, China
Corresponding author: Hong-yun ZHAO; Tel: +86-631-5687305; E-mail: shufengyuan@126.com
DOI: 10.1016/S1003-6326(15)63894-8

welded AA7A52 plates. The microstructure of the weld seam was composed of α(Al) and β(Mg_2Al_3), while the microstructure in the fusion zone was related to the fusion ratio. WU and WANG [8] tested the mechanical properties of the GTA welded AA7005 joints and found that the mechanical performances closely related to the ageing states. Fracture was found in the weld seam, the molten line and the HAZ for the samples subjected to 24 h, 110 °C ageing, natural ageing for 7 d and natural ageing for 14 d, respectively.

With regard to the numerical method, classical strength theories were adopted in the identification of the vulnerable zones. The fourth classical strength theory, as an universal strength theory to almost all kinds of materials, assessed the safety of materials by the shape change ratio of the cell body. Thus, the application of the fourth strength theory was converted to the solution of equivalent von Mises stress [9]. Failure of material and the corresponding judging criterion was also dependent upon the stress state of the material [10]. The maximum tensile stress theory, or the first classical strength theory, should be used for materials in the tri-axial tensile stress state. So, the fourth strength theory was independent of the stress state and suitable for assessing the reliability of the joint during welding process, while the first strength theory was suitable for assessing the reliability of the joint under working conditions. Few reports could be found upon the failure behavior of multi-pass cold-metal-transferring (CMT) welded joint. Moreover, even fewer references could be found about the influences of residual stress on the mechanical performances of the CMT welded joint. So, vulnerable zones in the multi-pass CMT welded joint were identified using the microstructure and numerical analysis in the present study. Vulnerable zones should be defined as the zones where cracks were easily initiated during the manufacturing process or under service conditions.

2 Experimental and FE model

The AA7A52 aluminum alloy plates with the dimensions of 100 mm × 100 mm × 20 mm were welded with cold-metal-transferring (CMT) process. The commercial ER5356 welding wire was used with pure argon as the shielding gas. The base coupons were degreased with acetone, cleaned with a brush that has stainless bristles, assembled along the weld joint and tacked. The joints were obtained by three-pass welding which is shown in Fig. 1. Samples for metallographic test were sectioned from the middle of the welded joint, mounted, mechanically polished and etched with standard Keller's reagent (2.5 mL HNO_3, 1.5 mL HCl, 1 mL HF and 95 mL deionized water).

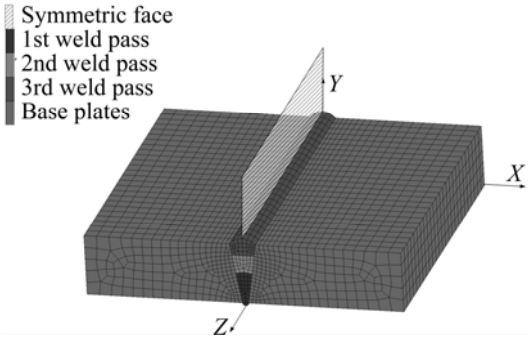

Fig. 1 Schematic diagram of welding process and location in Cartesian coordinates

A three-dimensional (3D) finite element (FE) model was developed, in which the elements of the weld seam and the adjacent zone were meshed to obtain smaller size. The elements were divided into four different parts including the base plates and three weld passes. The location of the model in the Cartesian coordinates is shown in Fig. 1. Modeling of the cooperation between wire feeding and heat input had been detailed in Ref. [11] together with the mechanical boundary conditions. The thermal boundary conditions and the thermal cycle had been analyzed [12], base upon which the thermal-mechanical analysis could be done in the present work. The distribution of final principal stresses was studied so as to assess the safety of the joint under working conditions, while evolution of the equivalent von Mises stress was studied for safety assessment during the welding process.

3 Results and discussion

3.1 Microstructure of joint

Firstly, special annotation should be given about fusion zone and molten zone. The former was used and referred to as the zone between the weld seam and the base plate, while the later was used to represent the zone between the weld passes.

The microstructures of the fusion zone and the center of the three weld passes are shown in Figs. 2 and 3, respectively. It was shown that grains in the first weld pass were like plum blossom, which should be due to the neoformative boundaries as a result of the precipitated solute from the matrix phase. In other words, grains in the first weld pass were refined by the subsequent weld passes via heat treatment. Although it was weaker in the second weld pass, the refinement was still revealed by the grain morphology in which the neoformative boundaries were shorter and less continuous. Grains in the third weld pass were coarser compared with that in the other weld passes.

Microstructures of the molten zone between the first

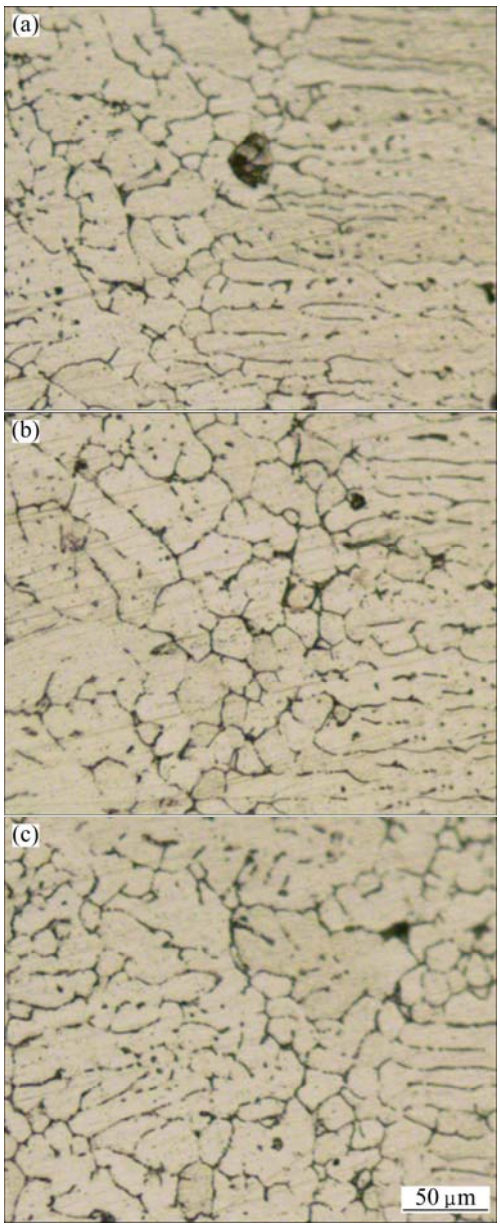

Fig. 2 Microstructures in fusion zone: (a) Between first weld pass and base metal; (b) Between second weld pass and base metal; (c) Between third weld pass and base metal

and the second weld passes are shown in Fig. 4(a) with the microstructure between the second and the third weld passes shown in Fig. 4(b). For the first weld pass the low-melting components were repelled to the weld seam boundary which should be remelted as a result of the second weld pass. The low-melting solution supplied a large number of nuclei for the following solidification process. Moreover, the remelted zone was the bottom of the molten pool where heat diffusion rate was the highest. As a result, grains in the remelted zone were refined. However, the remelted zone was also characterized with thicker grain boundary and more intergranular precipitates with low melting point. These components

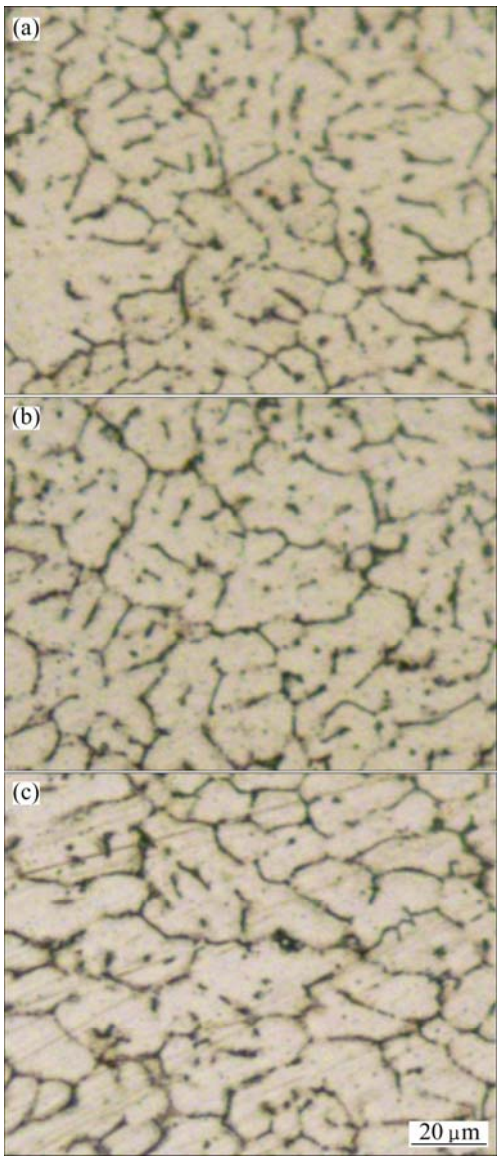

Fig. 3 Microstructures in center of three weld passes: (a) First weld pass; (b) Second weld pass; (c) Third weld pass

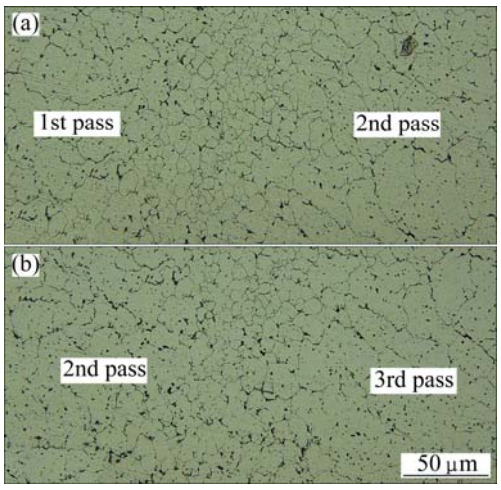

Fig. 4 Microstructure of molten zone: (a) Between first and second weld passes; (b) Between second and third weld passes

were firstly repelled to the upper surface of the former weld pass after solidification. Then, they were repelled to the grain boundaries during the solidification of the subsequent weld pass (or intergranular segregation), as a result, the coarse grain boundary was yielded. So, these zones with coarse microstructure were indicated to exhibit inferior mechanical performances.

3.2 Vulnerable zones of joint

Failure of the joint was interlocked to stress state of different zones. The first classical strength theory was therefore adopted for the safety evaluation of material under tri-axial tensile stress state, while the fourth classical strength theory was used for the other stress states. Tensile and compressive stresses were identified as positive and negative, respectively, in contour bands and distribution curves.

Contour bands of the principal stresses are shown in Fig. 5. It was shown that the zones under tri-axial tensile stress state included four corners under rigid fixation and fusion zone. Neither crystal crack nor hot crack was supposed to occur at the four rigidly fixed corners because of the relatively low peak temperature during its thermal cycling as detailed in Ref. [12]. Tri-axial tensile stress was found along the fusion zone resulting in tendency for tensile failure under working conditions, which was due to the compositional difference between both sides of the fusion line and got experimental supports [13]. The other vulnerable zone identified by the fourth strength theory was situated in the symmetric face, where the stress style was of tension-crush style, thus it was the sign of the principal stresses that made equivalent von Mises stress bigger than that along the fusion zone.

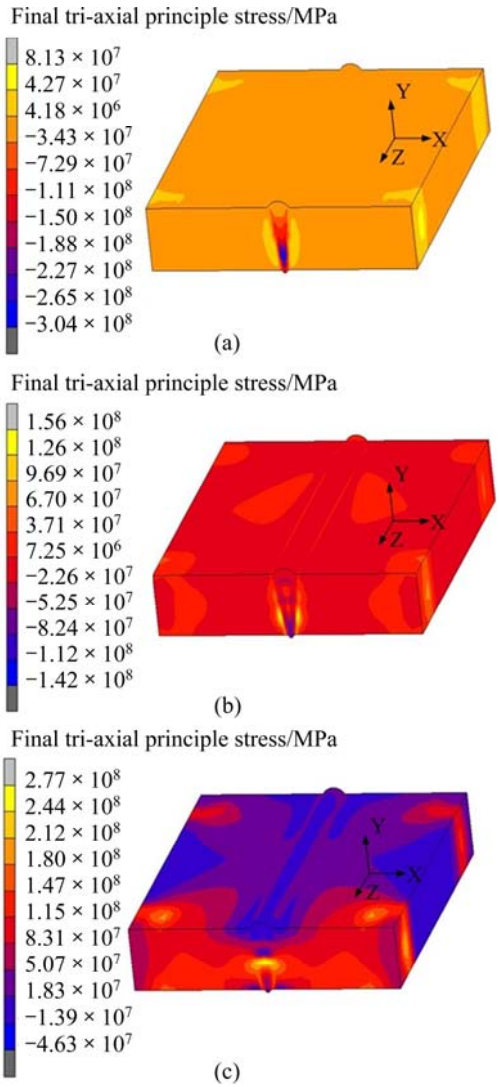

Fig. 5 Contour bands of final tri-axial principle stresses: (a) Minimum principal stress; (b) Intermediate principal stress; (c) Maximum principal stress

In order to accurately find the most vulnerable zone, the distribution of residual equivalent von Mises stress was studied along different lines in the symmetric face as shown in Fig. 6. The maximum residual equivalent von Mises stress zone transferred from the arc starting side to the arc ending side as the first weld seam was finished, as indicated by its distribution along line 2 (Fig. 7(b)). With regard to line 1, the peak value point transferred from the top of the weld seam (point *A*) to about 1 mm beneath (point *B*) which stayed as the peak point of line 1 till the end of the procedure. Stress distribution along line 2 was characterized by two peaks at both ends, and the peak value on the arc ending side was nearly twice that on the arc starting side. The maximum value along line 3 was found much smaller than that of line 1, as shown in Figs. 7(c) and (a). As conclusion, the top (point *A*) of the first weld pass at the arc ending side was regarded to be the most vulnerable. It was just before starting the second weld pass that the equivalent von Mises stress at point *A* was shown to be the highest.

Relativity between equivalent von Mises stress and transverse residual stress could be explained through the maximum principal stress. Figure 8 shows that distribution of the maximum principal stress was mainly dependent upon the first weld pass. Consistency was

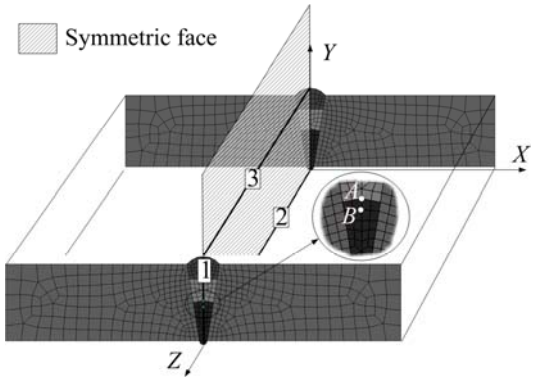

Fig. 6 Schematic of location of two specific points and specific lines along distribution of residual equivalent von Mises stress studied

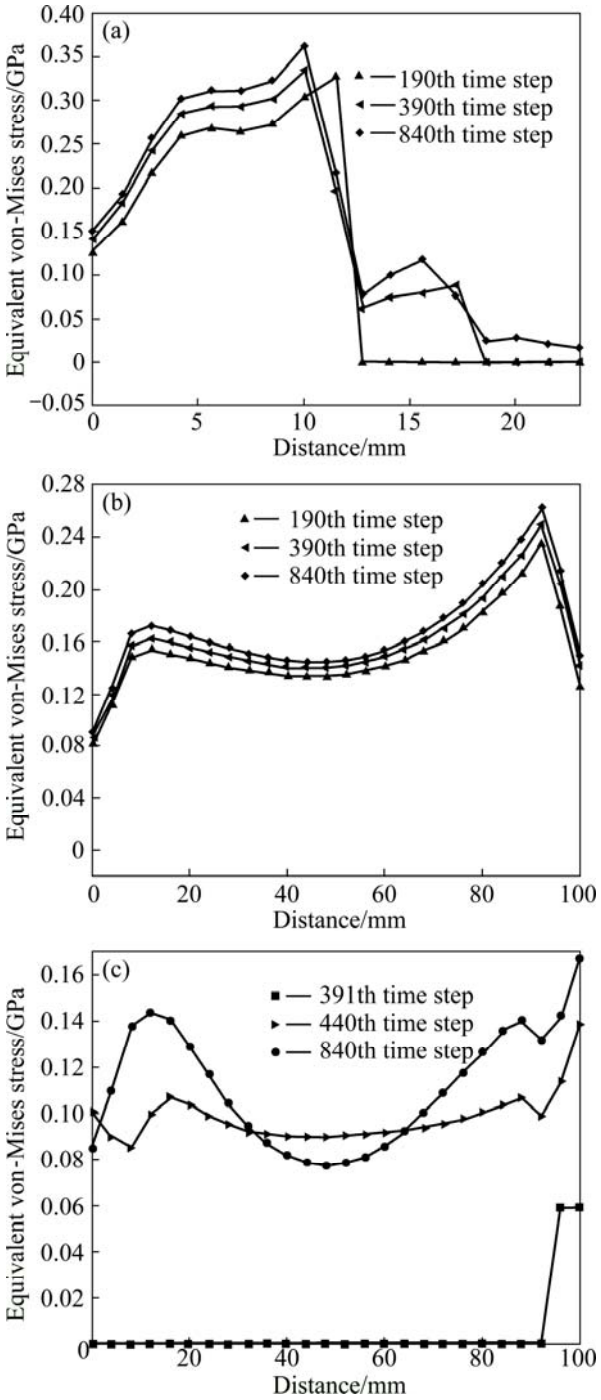

Fig. 7 Distribution of equivalent von Mises stress at different time steps: (a) Along line 1; (b) Along line 2; (c) Along line 3

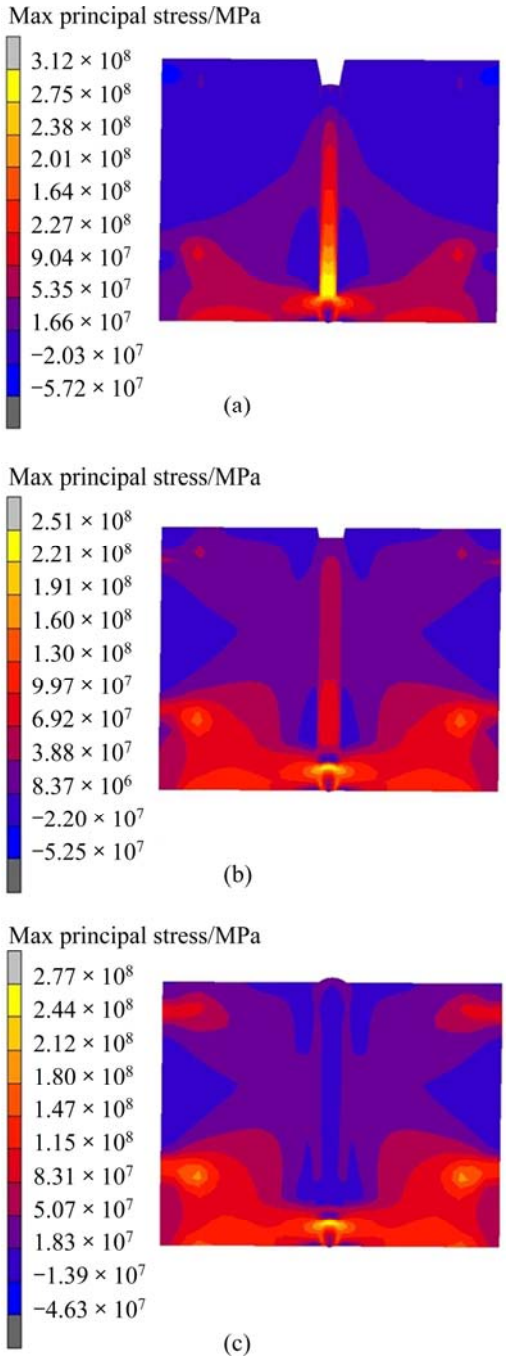

Fig. 8 Contour bands of maximum principal stress distribution on arc-ending side after every inter-pass cooling: (a) After 190th time step; (b) After 390th time step; (c) After 840th time step

found between evolution of the maximum principal stress and transverse residual stress through the comparison of Figs. 8 and 9. The highest tensile stress for every time step was the transverse stress [11], thus the maximum principal stress approximated transverse stress. So, it was appropriate to assess the vulnerable zone of the joint directly through transverse residual stress.

So, it was indicated by the microstructures of the joint that the vulnerable zone of the joint was located either in the center of the third weld pass or in the molten zone due to the coarse grain and the coarse grain boundary, respectively. As conclusion of the mechanical analysis, the residual stress distribution indicated that the most vulnerable zone in the joint was either the symmetric face of the joint or the boundaries between the weld seam and the base plates. The former was obtained under the conduction of the fourth classical strength theory, whereas the later under the conduction of the first

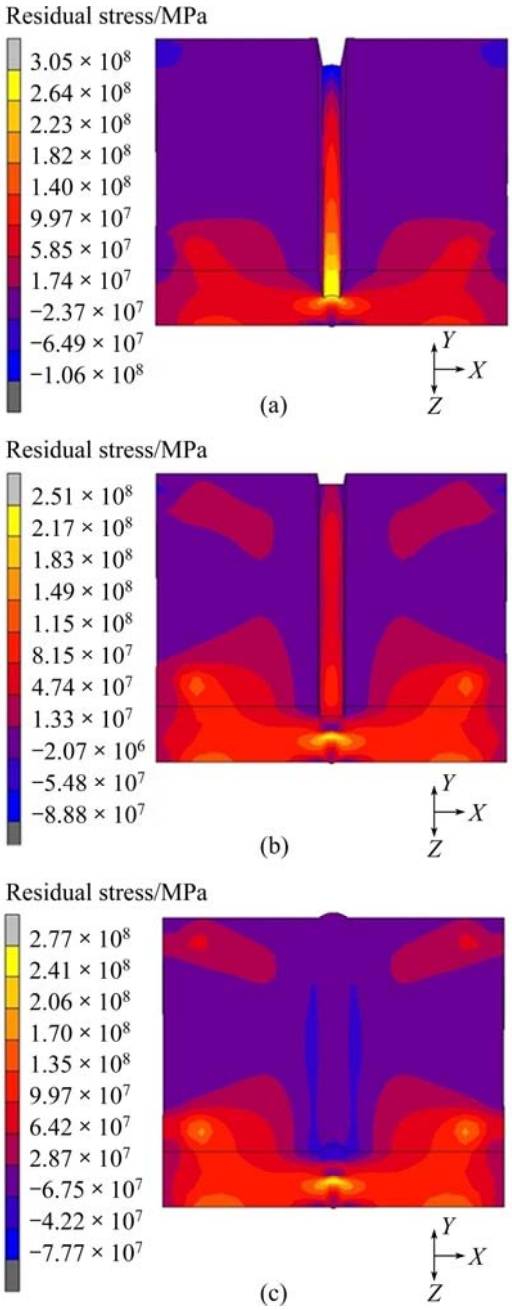

Fig. 9 Contour bands of transverse residual stress distribution after every inter-pass cooling: (a) After 190th time step; (b) After 390th time step; (c) After 840th time step

classical strength theory. The vulnerable zones identified by the presented work are shown in Fig. 10, which indicated that there were agreements between the judging results upon the zones highlighted with red dash lines. They were the crossed parts of the vulnerable zones, in other words, they were suggested to be the most vulnerable zones.

With regard to the welded Al−Zn−Mg alloys with ER5356 as filler metal, the prediction of breaking tendency in the symmetric face, the fusion zone and the molten zone had been proved by experimental research, respectively [13−15]. The third pass was indicated to have better ductility yet lower strength than the other passes, which resulted in unbalanced deformation in the tensile process. This meant that crack source was initiated in the other weld passes rather than the third weld pass. It was also indicated [14] that the local mechanical property was closely related to the compositional distribution, especially the zinc to magnesium content ratio. In addition, the plastic factors could be changed by material mismatch, which could lead to different crack locations [16]. Exactly, lots of work needed to be finished, such as numerical characterization of the fusion zone, optimization of the model and systematic research on the factors that influenced the mechanical properties of the multi-pass welded joint.

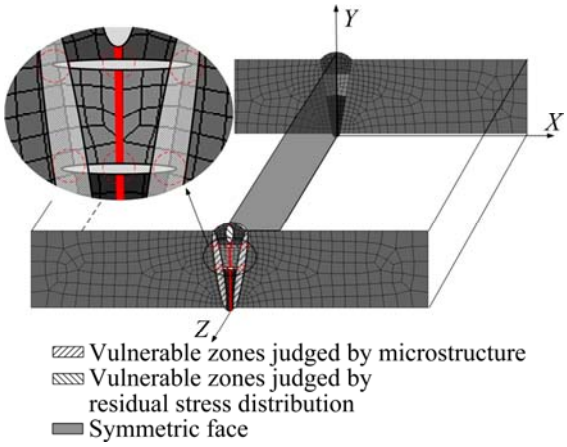

Fig. 10 Schematic of crossed parts in vulnerable zones identified by different methods

4 Conclusions

1) Grains were refined by the subsequent weld passes through heat treatment, as a result, the grain size in the third weld pass was the biggest. Intergranular segregation gave birth to the coarse grain boundary between the weld passes. These zones with coarse grain or grain boundary were indicated to exhibit inferior mechanical performances.

2) Tri-axial stress distribution in the fusion zone was indicative of tendency to tensile failure under service conditions. The top of the first weld pass at the arc-ending side was regarded to be vulnerable because the equivalent von Mises stress was the highest. Moreover, it made sense to assess the vulnerable zone of the joint directly through transverse residual stress.

3) The most vulnerable zones were regarded to be the crossed parts between the vulnerable zones which were identified according to the microstructure and the mechanical analysis.

References

[1] HUANG Ji-wu, YIN Zhi-min, LEI Xue-feng. Microstructure and properties of 7A52 Al alloy welded joint [J]. Transactions of Nonferrous Metals Society of China, 2008, 18(4): 804−808.

[2] PADDEA S, FRANCIS J A, PARADOWSKA A M, BOUCHARD P J, SHIBLI I A. Residual stress distributions in a P91 steel-pipe girth weld before and after post weld heat treatment [J]. Mater Sci Eng A, 2012, 534: 663−672.

[3] FU Gao-feng, TIAN Fu-quan, WANG Hong. Studies on softening of heat-affected zone of pulsed-current GMA welded Al−Zn−Mg alloy [J]. J Mater Process Tech, 2006, 180: 216−220.

[4] MA T, den OUDEN G. Softening behavior of Al−Zn−Mg alloys due to welding [J]. Mater Sci Eng A, 1999, 266: 198−204.

[5] YANG Dong-xia, LI Xiao-yan, HE Ding-yong, HUANG Hui. Effect of minor Er and Zr on microstructure and mechanical properties of Al−Mg−Mn alloy (5083) welded joints [J]. Mat Sci Eng A, 2013, 516: 226−231.

[6] MA Shi-ning, LOU Lin, LIU Qian, QIU Ji. Microstructure and properties of 7A52 aluminum alloy welded joints of different medium aqueous vapor plasma arc [J]. Mater Eng, 2010, 4: 36−41. (in Chinese)

[7] YU Jin, WANG Ke-hong, XU Yue-lan, LU Yong. Microstructures and properties of 7A52 aluminum alloy welded joint by twin wire welding [J]. Transactions of China Welding Institute, 2005, 26(10): 86−90. (in Chinese)

[8] WU Y E, WANG Y T. Enhanced SCC resistance of AA7005 welds with appropriate filler metal and post-welding heat treatment [J]. Theor Appl Fract Mec, 2010, 54: 19−26.

[9] LIU C, ZHANG J X, XUE C B. Numerical investigation on residual stress distribution and evolution during multipass narrow gap welding of thick-walled stainless steel pipes [J]. Fusion Eng Des, 2011, 86: 288−295.

[10] QU Feng-sheng, LIU Xu-guang, XING Fei, ZHANG Kai-feng. High temperature tensile properties of laser butt-welded plate of Inconel 718 superalloy with ultra-fine grains [J]. Transactions of Nonferrous Metals Society of China, 2012, 22(10): 2379−2388.

[11] SHU Feng-yuan, LV Yao-hui, LIU Yu-xin, SUN Zhe, HE Peng, XU Bin-shi. Residual stress modeling of narrow gap welded joint of aluminum alloy by cold metal transferring procedure [J]. Constr Build Mater, 2014, 54: 224−235.

[12] SHU Feng-yuan, LÜ Yao-hui, LIU Yu-xin, XU Fu-jia, SUN Zhe, HE Peng, XU Bin-shi. FEM modeling of softened base metal in narrow-gap joint by CMT+P MIX welding procedure [J]. Transactions of Nonferrous Metals Society of China, 2014, 24(6): 1830−1835.

[13] HUANG Ji-wu, YIN Zhi-min, WAN Jia-fang, NIE Bo, HE Zhen-bo. Effect of homogenization treatment on microstructure and properties of 7A52 aluminum alloys [J]. J Cent South Univ, 2006, 36(6): 1070−1074.

[14] SHU Feng-yuan, LV Yao-hui, LIU Yu-xin, SUN Zhe, XU Bin-shi. Effects of different filler metals on the mechanical behaviours of GTA welded AA7A52 (T6) [J]. J Mater Eng Perform, 2014, 23(6): 2293−2299.

[15] BALASUBRAMANIAN V, RAVISANKAR V, MADHUSUDHAN R G. Influences of pulsed current welding and post weld aging treatment on fatigue crack growth behaviour of AA7075 aluminum alloy joints [J]. Int J Fatigue, 2008, 30(3): 405−416.

[16] KOO J M, HUH Y, SEOK C S. Plastic η factor considering strength mismatch and crack location in narrow gap weldments [J]. Nucl Eng Des, 2012, 247: 34−41.

基于残余应力和微观组织形貌的铝合金 CMT 焊接接头薄弱环节的预测

舒凤远[1,2]，田 泽[1]，吕耀辉[2]，贺文雄[1]，吕飞洋[1]，林建军[2,3]，赵洪运[1]，徐滨士[2]

1. 哈尔滨工业大学(威海) 材料科学与工程学院，山东省特种焊接技术重点实验室，威海 264209；
2. 装甲兵工程学院 再制造技术国防科技重点实验室，北京 100072；
3. 上海交通大学 材料激光加工与改性上海市重点实验室，上海 200240

摘 要：采用数值模拟与实验相结合的方法预测 3 道冷金属过渡(CMT)焊接接头的薄弱环节。通过有限元方法预测焊接接头中残余应力的分布特征；通过金相实验获得焊接接头中不同特征区域的微观组织形貌特征。接头对称面上的最大主应力值最高，故该区域在服役过程中较易产生拉伸裂纹。第一次层间冷却结束后，焊缝金属与基板的交界面上因等效 von-Mises 应力最大而具有较高的裂纹敏感性。根据金相分析结果，第 3 道焊缝中晶粒最为粗大，而层间的熔合区则具有粗大的晶间析出物组织特征，两种现象均意味着较差的力学性能。焊接接头中最为薄弱的区域则位于分别通过数值方法和实验方法得出的薄弱区域的交叉区域。

关键词：铝合金；薄弱环节；冷金属过渡(CMT)焊接接头；残余应力；组织形貌

(Edited by Xiang-qun LI)